Original Paper

Fixed- and variable-frequency sliding mode controller–maximum power point tracking converter for two-stage grid-integrated photovoltaic system employing nonlinear loads with power quality improvement features

Ravichandran Chinnappan[1] , Premalatha Logamani[2] and Rengaraj Ramasubbu[3]

Abstract
This article presents a reliable and efficient photovoltaic sliding mode voltage-controlled maximum power point tracking DC-DC converter–active power filter integration system to supply real power to grid. This integrated active power filter system performs power quality enhancement features to compensate current harmonics to make distortion-free grid supply current and reactive power employing nonlinear loads. The proposed proportional–integral–derivative–based sliding mode controller is designed with fixed-frequency pulse-width modulation based on equivalent control approach. The main objective of this paper is to design a photovoltaic system with a new sliding surface to force the photovoltaic voltage to follow the reference maximum power point voltage with the alleviation of slow transient response and disadvantages of chattering effects of variable-frequency hysteresis modulation sliding mode controller–maximum power point tracking. The perturbations caused by the uncertainties in climatic conditions and converter output bulk oscillations during grid integration are also mitigated. The features of the proposed photovoltaic–active power filter integration system are confirmed at different operating conditions through PSIM simulation software, and its performance is also compared with a conventional variable-frequency sliding mode-controlled maximum power point tracking. The obtained simulation and experimental results give good dynamic response under various operating conditions of environmental and local load conditions.

Introduction

Nowadays, the integration of renewable energy sources at distribution level called distribution generation (DG) is becoming a challenging technology due to global warming, green house gas emission and environmental contamination.[1–3] Recently, among the various types of DG system, two-stage grid-integrated photovoltaic (PV) system especially microinverter (PV module-integrated converter) becomes more popular because of its own maximum power point tracking (MPPT) capabilities, cost reduction in end-users, simplified system installation and fulfilment of voltage gain requirement.[4–6] However, in two-stage PV system, the dynamic interaction among the DC-DC converter, inverter and

MPPT controller may decrease the system performances in terms of system efficiency and confused in voltage-oriented MPPT techniques, for example,

[1]Department of Electrical and Electronics Engineering, Anand Institute of Higher Technology, Kazhipathur, Tamil Nadu, India
[2]School of Electrical Engineering, Vellore Institute of Technology, Chennai, India
[3]Department of Electrical and Electronics Engineering, SSN College of Engineering, Chennai, Tamil Nadu, India

Corresponding author:
Ravichandran Chinnappan, Department of Electrical and Electronics Engineering, Anand Institute of Higher Technology, Kazhipathur, Tamil Nadu 603103, India.
Email: cravichandran0903@gmail.com

perturb and observe (P&O) method. This is mainly due to PV voltage oscillations caused by the second harmonic frequency of the grid[7] and nonlinear characteristics of PV cells depending on irradiance and temperature.[8] Among the various solution methods proposed in grid-integrated PV system to mitigate such voltage oscillations, the most preferable and the first alternative is a linear proportional–integral (PI) + pulse-width modulation (PWM), proportional–integral–derivative (PID) + PWM or peak current mode + PWM controller. These controllers ensure stability with the ability to track the PV voltage reference generated by the MPPT algorithm under uncertainties in load perturbations and climatic conditions.[7,9,10] However, the main problem associated with these controllers is loss of stability due to low-frequency sinusoidal voltage perturbations imposed by the grid in the DC bus. Thus, the necessity of linearizing the model of PV system arises to ensure same performances in all the operation ranges.[2,3,11] Focusing the nonlinear controllers, particularly sliding mode controllers (SMCs), is a better candidate than conventional linear controllers for mitigating such low-frequency oscillations and load perturbations due to their excellent characteristics of stability, simpler implementation and robustness against parameters which are common in PV system.[4,12,13] However, SMC approach applied to MPPT DC-DC converter has certain limitations in the design of filter circuit due to variable operating frequency and high chattering magnitude such as PV voltage fluctuations. Hence, to ensure stability of a voltage-oriented MPPT algorithm with fast settling time, alleviating high chattering magnitude and mitigating low-frequency oscillations of the PV voltage especially in grid-connected environment, the necessity of constant frequency operation of SMC-MPPT converter is an important one in this concern.[14–16]

This paper proposes a design procedure of PID-based sliding mode (SM) voltage controller for PV-MPPT application. The discussion of SM control theory based on variable-frequency hysteresis modulation and equivalent control approach based on fixed-frequency PWM duty ratio concept is focused in this paper. The dynamic state-space modelling method for designing SM voltage-controlled MPPT high step-up DC-DC converter in terms of the desired control variable (i.e. voltage) is outlined in this regard. The introduction of voltage error integral term in the control computation is to reduce the steady-state PV voltage error of the SM-controlled system.

With prevalent increase in power electronic equipments and use of nonlinear loads at the point of common coupling (PCC), current and voltage distortion is produced in distribution grid which affects the quality of power.[2] To maintain good quality of power at PCC, various national and international agencies have released standards and guidelines that specify limits on the magnitudes of harmonic distortion in currents and voltages.[17] In order to provide harmonic-free grid

supply current, the solution is the use of active power filter (APF) technology having better compensation characteristics to inject harmonic current with suitable magnitude and phase into the PCC. In most of the literatures, control strategy of inverter in grid-connected mode concentrates only on injecting active power to the grid and not on power quality functions employing nonlinear loads such as compensating harmonics and reactive power drained by local loads, particularly APF integration functionality.[3,10]

The main contribution of this paper is to provide the effective integration of PV energy source into the distribution grid with power quality features that can be done by constant-frequency SMC-MPPT high step-up DC-DC converter[6,5,18,19] connected with grid-interfacing inverter. With the aid of MPPT converter, the possibility of faster response in P&O MPPT control variable has superior tracking performances of PV in the poor atmospheric conditions. The grid-interfacing inverter has additional features of shunt active power filtering capability without additional cost of implementation and performs good power quality features at PCC feeding a various linear and nonlinear loads.[8,11] SMC-MPPT DC-DC converter connected with grid-interfacing inverter will act as microinverter with active filtering capability to compensate the low-frequency voltage ripple on the DC-side of the PV system.[20,21]

The entire features can be done by either separately or simultaneously with suitable control of inverter. A simple and cost-effective nonlinear control scheme is applied to the control of single-phase grid inverter.[22] The inner current controller used is based on SMC to force the current of the inverter to track their reference value. The suggested SM control of inverter and MPPT converter has been found to be practicable, cost-effective and excellent compensation characteristics especially in low- and medium-scaled PV systems.

The proposed PV-APF integration system is simulated in PSIM environment for different operating conditions of loads and uncertainties in climatic condition. The transient and steady-state performances of proposed fixed-frequency PWM-based SMC-MPPT configuration can be compared with variable-frequency hysteresis modulation-based SMC-MPPT configuration.

Description of system configuration

The configuration of the proposed double-stage PV-APF combination system using variable- and fixed-frequency SMC-MPPT converter is shown in Figures 1 and 2, respectively. The PV module is connected to the DC-DC converter in which boost, flyback and forward operation are integrated on a single magnetic core to achieve high step-up voltage with low duty ratio. The operation of high step-up DC-DC converter is based on command signal derived from SM controller with voltage-oriented P&O MPPT technique implemented to extract maximum PV power. The main objective of

the proposed SM controller is to provide good dynamic response of PV system under variation of environmental, load uncertainties, sinusoidal oscillations imposed by the grid and to ensure the accurate tracking of reference PV voltage provided by the MPPT algorithm.[7,8] The nonlinear load which is constructed using full-bridge diode rectifier with a smoothing inductor and DC filter capacitor connected to the grid is considered as a step change in load. The single-phase H-bridge inverter is connected between the MPPT converter and the distribution grid. The integration of APF functionality in grid inverter needs a particular attention for the generation of reference current and design of controller. The nonlinear controller based on SMC law is used to implement the voltage and current controller of the inverter.

The functions that can be carried out by the inverter controller are as follows:

1. The control of active power flow from PV source to PCC;
2. Compensation of reactive power demanded by the load and the nonlinear load current harmonics, keeping the distortion-free sinusoidal grid supply current.

In the daytime with availability of PV energy, the PV-APF combination system brings all its functions into operation. During nighttime and no sunlight periods, the power required by the local loads is consumed from the grid source while the inverter system performs shunt active power filtering function to compensate harmonic currents and reactive power. Thus, the utilization level of the PV-APF combination is higher than the conventional grid interactive PV inverter system.

Gain of the high step-up DC-DC converter

From steady-state operating modes of DC-DC converter (see Figures 1 and 2), the voltage developed across the capacitor C_3 is derived as equal to the output voltage of conventional boost converter[18]

$$V_{C_3} = \frac{1}{1-d} V_{PV} \tag{1}$$

where d is the duty cycle of converter.

Due to flyback operation of coupled inductor, the voltage developed across the output capacitor C_1 is derived as
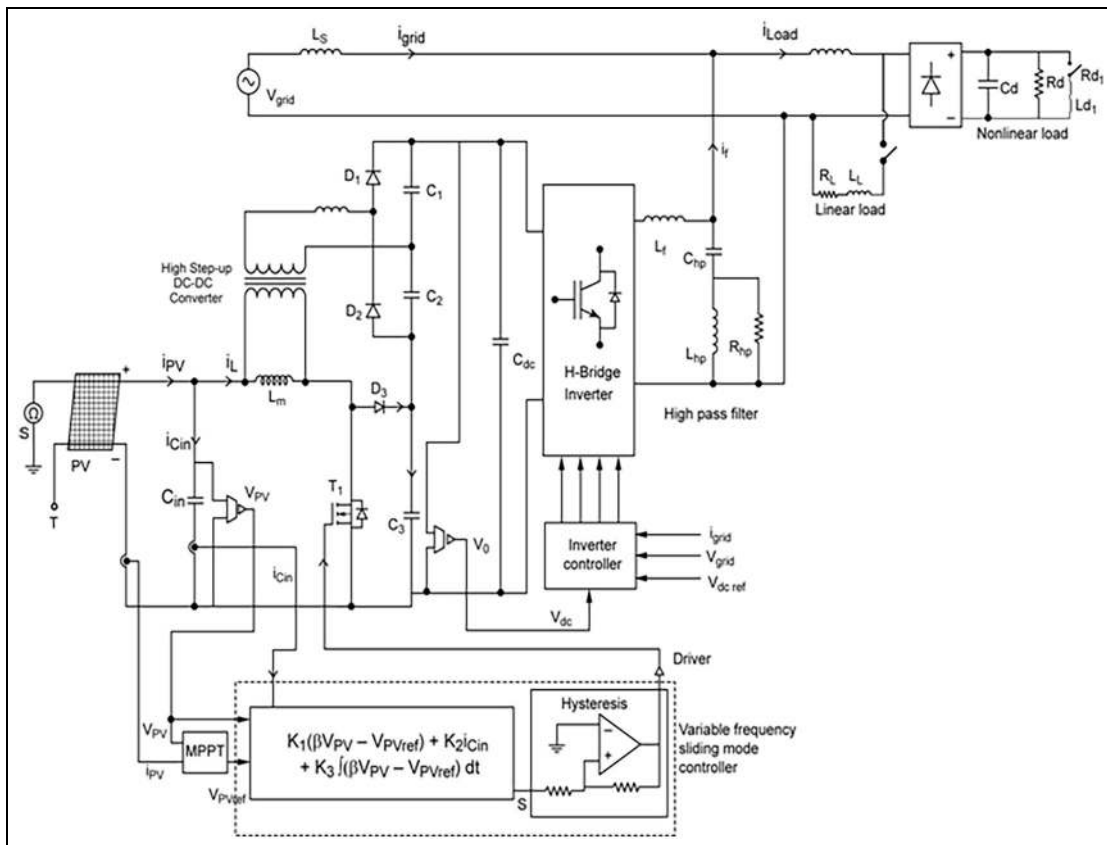
$$V_{C_3} = nV_{PV} \frac{d}{1-d} \tag{2}$$

Figure 1. Configuration of PV-APF combination system employing variable-frequency hysteresis modulation-based SMC-MPPT converter.
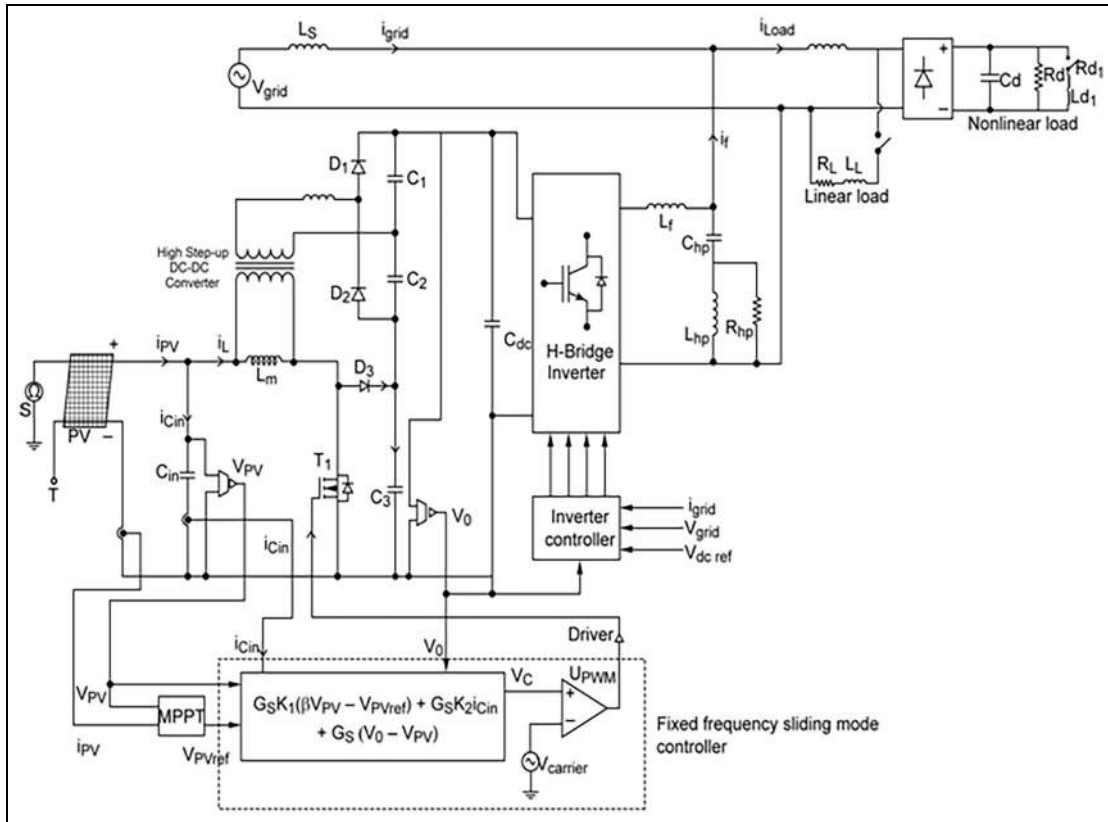
Figure 2. Configuration of PV-APF combination system employing fixed-frequency PWM-based SMC-MPPT converter.

Due to forward operation of coupled inductor, the voltage developed across the output capacitor C_2 is derived as

$$V_{C_2} = nV_{PV} \tag{3}$$

Thus, due to the series connection nature of C_1 and C_2, the resultant output voltage is a function of boost converter with multiplication factor of 'n'

$$V_{C_1} + V_{C_2} = nV_{PV} + \frac{nd}{1-d}V_{PV} = \frac{n}{1-d}V_{PV} \tag{4}$$

This voltage is added with the boost converter output voltage and resultant output voltage can be derived as $V_o = V_{C_1} + V_{C_2} + V_{C_3} + V_{C_4}$

$$V_o = \frac{V_{PV}}{1-d}(1+n) \tag{5}$$

Variable-frequency hysteresis modulation-based SM-controlled MPPT converter

The general SM control law of DC-DC converter employing single switch to adopt a switching function is given as

$$u = \frac{1}{2}(1 + sign(S)) \tag{6}$$

where u is the logic state of DC-DC converter power switch T_1 and S is the instantaneous state variable's trajectory treated as sliding surface.

The usual method of implementing the SM controller based on the control law described in Equation (6) is realized easily by switch relay and through an analogue or digital computational circuit. However, the direct implementation of this control methodology results in unpredictable frequencies which are not suitable for the control purpose of the converters.

One of the most popular techniques of operating frequency in a controllable way is hysteresis modulation. This method does not concern about additional computational circuitries, and its implementation can be done simply by defining the logic state of power switch T_1 as

$$u = \begin{cases} 0 = off & \text{when } S > h \\ 1 = on & \text{when } S < -h \end{cases} \tag{6a}$$

and the sliding surface S is

$$S = \alpha_1 y_1 + \alpha_2 y_2 + \alpha_3 y_3 \tag{7}$$

where h is a fixed parameter and is an arbitrarily small value, and α_1, α_2 and α_3 represent the sliding coefficients which act as the desired control parameters. The introduction of a hysteresis band value of $2h$ with the boundary conditions $S = h$ and $S = -h$ controls the switching frequency of the converter along with practical requirement of a switching operation.

The controlled state variables are expressed as

$$y_1 = \beta v_{PV} - V_{PVref}$$
$$y_2 = \frac{d(\beta v_{PV} - V_{PVref})}{dt} = \beta \frac{i_{cn}}{c_{in}} \quad (8)$$
$$y_3 = \int (\beta v_{PV} - V_{PVref}) dt$$

where V_{PVref} is the reference value of PV voltage, V_{PV}, derived from the voltage-oriented MPPT control and β is the scaling factor.

Using Equations (7) and (8)

$$S = \alpha_1 (\beta v_{PV} - V_{PVref}) + \alpha_2 \frac{\beta}{c_{in}} i_{cn}$$
$$+ \alpha_3 \int (\beta v_{PV} - V_{PVref}) dt \quad (9)$$

Equation (9) directly relates

$$S = K_1 (\beta v_{PV} - V_{PVref}) + K_2 i_{cn}$$
$$+ K_3 \int (\beta v_{PV} - V_{PVref}) dt$$

where the gain parameters are

$$K_1 = \alpha_1; \quad K_2 = \alpha_2 \frac{\beta}{c_{in}}; \quad K_3 = \alpha_3$$

The realization of variable-frequency hysteresis SM operation can easily be achieved by implementing control Equation (9) into a controller (see Figure 1). The gating signal is generated using Schmitt trigger–type hysteresis comparator. In general, due to the presence of hysteresis band in switching function, an error will be introduced in the PV voltage. So, it is essential to select the hysteresis band h to a small value to minimize this error. Furthermore, if h is too small, it may be very sensitive to change in frequency. But if the hysteresis band is kept wide, the switching frequency can be limited to a consistent value depending on the requirements of power semiconductor switching. Hence, the gating signal generated using Schmitt trigger–type hysteresis comparator is provided with hysteresis band of $0.02 \leqslant h \leqslant 0.2$ to satisfy both the requirements. Thus, it is essential to make conventional variable-frequency SMC for PV-MPPT application to operate at fixed frequency and it should be considered seriously.

Fixed-frequency PWM-based SM-controlled MPPT converter

The discrete gate signal u in variable-frequency hysteresis modulation can be replaced by a smooth function called the equivalent control signal u_{equ} which is effectively based on the duty cycle control concept of pulse-width-modulated DC-DC converter.[16]

The time differentiation of Equation (7) to zero gives the equivalent control signal of the proposed fixed-frequency SM controller as

$$\dot{S} = \alpha_1 \dot{y}_1 + \alpha_2 \dot{y}_2 + \alpha_3 \dot{y}_3 = 0 \quad (10)$$

The time differentiation of Equation (8) gives the dynamic model of the proposed system derived as

$$\dot{y}_1 = \frac{d(\beta v_{PV} - V_{PVref})}{dt} = \frac{\beta}{C_{in}} i_{Cin}$$
$$\dot{y}_2 = \frac{\beta}{C_{in}} \frac{d}{dt} i_{Cin} = \frac{\beta}{C_{in}} \frac{d}{dt} (i_{PV} - i_{Lm})$$
$$= \frac{\beta}{r_{PV} C_{in}^2} i_{Cin} - \frac{v_{PV} - (1-u)v_0}{L_m} \quad (11)$$
$$\dot{y}_3 = \beta v_{PV} - V_{PVref}$$

where r_{PV} is the dynamic resistance of the panel and v_0 is the output voltage of the DC-DC converter.

The control signal of the proposed SMC based on equivalent control approach is derived by solving Equation (10) and inequality $0 < u = u_{equ} < 1$ and multiplying with v_0 gives

$$o < u_{equ} = \frac{\alpha_3 LC_{in}}{\alpha_2} (\beta v_{PV} - V_{PVref})$$
$$+ L \left(\frac{\alpha_1}{\alpha_2} + \frac{1}{C_{in} r_{PV}} \right) i_{Cin} + v_0 - v_{PV} < v_o \quad (12)$$

The control signal v_c is needed for implementing the fixed-frequency SMC-MPPT using duty ratio control concept d, where $0 < d = (v_c / v_{carrier}) < 1$ gives

$$v_c = G_s K_1 (\beta v_{PV} - V_{PVref}) + G_s K_2 i_{Cin} + G_s (v_o - v_{PV})$$
$$v_{carrier} = G_s v_o \quad (13)$$

where the gain parameters of the proposed controller are as follows

$$K_1 = \frac{\alpha_3 LC_{in}}{\alpha_2}$$
$$K_2 = L \left(\frac{\alpha_1}{\alpha_2} + \frac{1}{C_{in} r_{PV}} \right)$$

A suitable scaling factor G_s is introduced to scale down the magnitude of voltage signal into standard chip-level signal. The realization of fixed-frequency PWM-based SM operation can be achieved easily by implementing control Equation (13) into a controller (see Figure 2). The gating signal is generated by comparing v_c with $v_{carrier}$ using PWM comparator.

Selection of sliding coefficients

The choices of sliding coefficients based on the desired dynamic properties are made using Ackermann's formula.[16] Hence, the equation governing the sliding coefficients for the transient response of the converter during SMC-MPPT operation can be easily determined by substituting $S = 0$ in Equation (7) which results in a linear second-order equation
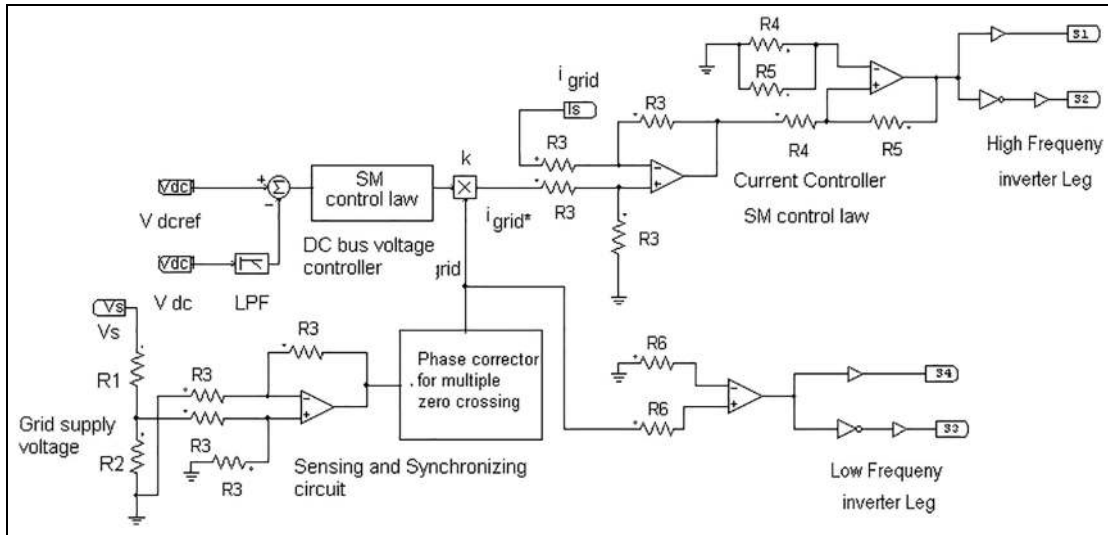
Figure 3. Inverter control scheme.

$$\alpha_1 y_1 + \alpha_2 \frac{d}{dt} y_1 + \alpha_3 \int y_1 dt = 0$$

$$\frac{d^2}{dt^2} y_1 + 2\sigma\omega_n \frac{d}{dt} y_1 + \omega_n^2 y_1 = 0 \tag{14}$$

where $\sigma = \frac{\alpha_1}{2\sqrt{\alpha_2 \alpha_3}}$ is the damping ratio and $\omega_n = \frac{\alpha_3}{\alpha_2}$ is the undamped natural frequency. In critically damped condition, considering damping ratio $\gamma = 1$, the following design equations are obtained

$$\frac{\alpha_1}{\alpha_2} = 4\pi f_{BW}$$

$$\frac{\alpha_3}{\alpha_2} = 4\pi^2 f_{BW}^2 \tag{15}$$

Thus, the design of the sliding coefficients depends on the bandwidth f_{BW} of the desired frequency response. According to Equations (13) and (15), the control parameters obtained are $K_1 = 1$ and $K_2 = 10$ for the 1-kHz bandwidth of the controller.

Inverter control strategy and model

The control scheme of the grid-interfacing inverter is shown in Figure 3. It consists of inner-loop current controller, outer-loop voltage controller and modulation scheme. The principle scheme of inner-loop current controller is by forcing the grid supply current i_{grid} always sinusoidal and in phase with the grid supply voltage v_{grid}. Therefore, the defined control objective of grid supply current can be expressed as

$$i_{grid}^* = kv_{grid} \tag{16}$$

where i_{grid}^* is the reference grid supply current and k is the scaling factor given by an outer-loop voltage controller which accounts for the real power consumed by the nonlinear loads. The value of k is derived from an outer-loop PI voltage controller.

A standard form of simple sliding surface, ψ, is defined using the grid supply current error as

$$\psi = kv_{grid} - i_{grid} = 0 \text{ or } \psi = i_{grid}^* - i_{grid} \tag{17}$$

Practically, the voltage at the PCC is distorted due to the presence of source impedance and nonlinear current flowing through it. Such supply systems are represented as weak or non-stiff sources. When compensation is applied to non-stiff sources, the PCC voltage may have multiple zero crossings due to the switching harmonics in the grid supply current and at such circumstances, it is difficult to extract zero crossing instance of the PCC voltage. So, it is important to detect the zero crossing instants of the voltage to attain reliable operation of the grid inverter functioning as an APF. Conventionally, a phase-locked loop (PLL) is used to create unity sinusoidal voltage in synchronization with grid inverter.[23–25] However, due to inherent delay in the PLL, the transient response of the grid inverter is affected. Newly developed single-phase PLL structures and its high-performance features are reported in several publications.[26–29] However, such schemes cannot be easily implemented due to the complexity in different way of presentations and lack of comprehensive knowledge about their dynamic features and stability.

In this work, the simple and low-cost grid synchronization circuit is designed particularly for a low-scaled, two-stage grid-integrated PV system which is a combination of low-pass filter (LPF) and phase corrector. The sensed and scaled PCC voltage is passed to LPF which is designed for extracting the 50-Hz fundamental frequency component. The phase shift introduced by the LPF is corrected using phase corrector (which consists of an adjustable resistor that can be used to adjust the value of phase shift). The phase corrector output signal is used to synchronize the operation of grid inverter with PCC voltage. With the presented synchronization circuit, proper sequencing of the operation of grid

Table 1. SMC law for grid inverter.

	$i_{grid} < kv_{grid}$ $V_{grid} < 0$	$i_{grid} > kv_{grid}$ $V_{grid} > 0$
u_1	0	1
u_2	1	0
u_3	1	0
u_4	0	1

inverter can be attained even under the multiple zero crossings of grid supply voltage.

The nonlinear control law used to implement the current controller of inverter is stated in Table 1. Usually, the SM control law which forces the grid supply current to track the reference current can be expressed as

$$u_x = \begin{cases} 0 = off & \text{when } \psi > \delta \\ 1 = on & \text{when } \psi < -\delta \end{cases} \quad (18)$$

where δ is a fixed parameter and is an arbitrarily small value. The introduction of a hysteresis band value of 2δ with the boundary conditions $\psi = \delta$ and $\psi = -\delta$ controls the switching frequency of the converter with practical requirement of switching operation. The SMC law in Table 1 is implemented with a Schmitt trigger–type hysteresis current controller (shown in Figure 3) to generate unipolar hysteresis control pulses for inverter switches. To implement unipolar hysteresis modulation, switches S_3 and S_4 (operated as low-frequency leg) are controlled by the synchronization signal of the grid voltage and switches S_1 and S_2 (operated as high-frequency leg) are controlled by the error signal of the grid current. As a result, three levels of voltage ($+V_{dc}$, $-V_{dc}$ and 0) are generated at the output of inverter with low switching ripples.

The grid inverter used in APF topology is operated in current-controlled voltage source inverter (CCVSI) which uses DC bus capacitor as the supply and switches at high frequency to generate a necessary compensation current that follows the current reference equal to the reactive load current and harmonic load current. From inverter controller scheme shown in Figure 3, the DC bus capacitor voltage, V_{dc}, is measured and filtered through a LPF to yield average capacitor voltage with a cut-off frequency lower than twice the grid supply frequency to make reduced harmonic content in the reference current. The short-cut frequency of the LPF is approximately 88 Hz, which is lower than twice the grid supply frequency. This measured voltage is compared with the reference DC bus voltage V_{dcref}. Usually, the error signal thus obtained is given to a PI-type voltage controller to maintain a constant DC-link voltage, V_{dc}, and controls the exchange of active power between PV source and grid under varying conditions of load and PV power.[30] Thus, the voltage across the DC bus capacitor, C_{dc}, must be kept to a value that is higher than

the amplitude of the grid source voltage, $> \sqrt{2}V_{grid}$, to assist the active and reactive power flow. The minimum voltage calculated using this relation is 155 V. Hence, the voltage level of 180 is chosen for this system. The MPPT DC-DC converter gain should also satisfy this voltage-level criterion.

Hence, the output of the PI voltage controller, k, is defined as

$$k = K_p(V_{dcref} - V_{dc}) + K_i \int (V_{dcref} - V_{dc})dt \quad (19)$$

where K_p is the proportional gain that determines the dynamic response of DC bus voltage and K_i is the integral gain that determines its settling time. The proper choices of K_p and K_i are essentially important criteria to satisfy these control performances.

The PI voltage controller is replaced with the PID-SM voltage controller to achieve the fast dynamic response similarly as in Equation (8)

$$\begin{aligned} z_1 &= V_{dcref} - \beta v_{dc} \\ z_2 &= \frac{d(V_{dcref} - \beta v_{dc})}{dt} \text{ or } z_2 = -\beta \frac{i_{dc}}{c_{dc}} \\ z_3 &= \int (V_{dcref} - \beta v_{dc})dt \end{aligned} \quad (20)$$

Hence, the derived sliding surface of the voltage controller is

$$\begin{aligned} S(k) &= K_p\big(V_{dcref} - V_{dc}\big) - \beta \frac{i_{dc}}{c_{dc}} \\ &+ K_i \int \big(V_{dcref} - V_{dc}\big)dt \end{aligned} \quad (21)$$

The SMC-MPPT converter collects maximum available power from PV source and feeds into the DC bus of the grid-interfacing inverter. Hence, the DC bus plays a very important role in supplying this unpredictable nature of power from PV source to the grid.

The current, I_{dc}, derived from converter into DC-link with a voltage level, V_{dc}, can be given as

$$I_{dc} = \frac{P_{dc}}{V_{dc}} \quad (22)$$

where P_{dc} is the converter output power extracted from PV source. Simultaneously, the current flowing from DC bus to inverter can be given as

$$I_{dcin} = \frac{P_i}{V_{dc}} = \frac{(P_{inv} + P_l)}{V_{dc}} \quad (23)$$

where P_{inv} is the active power supplied to grid available at inverter output, P_i is the power available at the input of inverter and P_l is the losses incurred in inverter.

The two switches in each leg of H-bridge inverter must operate in complementary manner. This ensures that at any time, one switch will be conducting and simultaneous conduction of two switches is prohibited.

Table 2. List of components.

S. No	Components	Specifications/values
1.	Maximum power output of PV panel, P_{max}	100 W
2.	Open circuit voltage, V_{OC}	20.7 V
3.	Short circuit current, I_{SC}	6.3 A
4.	Voltage at MPP, V_{MPP}	17 V
5.	Current at MPP, I_{MPP}	5.83 A
6.	Reference PV voltage, VPV_{ref}	15–17.2 V
7.	Grid supply system	Single-phase 230 V/110 V, 50 Hz
8.	DC bus voltage reference, V_{dcref}	180 V
9.	Filter inductor, L_f	2 mH
10.	DC bus capacitor, C_{dc}	2000 μF
11.	Input PV capacitor, C_{in}	47 μF
12.	Capacitor C_1, C_2, C_3	100 μF, 100 μF, 470 μF
13.	Magnetizing inductor, L_m	500 μH
14.	Power switch T_1 (MOSFET)	IRFP 250
15.	MOSFET driver IC	IR2110
16.	Diodes D_1, D_2, D_3	MUR1560
17.	Switching frequency	100 kHz
18.	Carrier amplitude	2 V
19.	Controller ICs	CA 3140, LF 347

PV: photovoltaic; MPP: maximum power point.

This represents

$$u_1 + u_2 = 1$$
$$u_3 + u_4 = 1 \quad (24)$$

The average modelling of generated inverter output voltage, V_{inv}, in terms of instantaneous DC bus voltage, V_{dc}, and state 'u_x' can be given as

$$V_{inv} = (u_1 u_4 - u_2 u_3)V_{dc} \quad (25)$$

Similarly, the charging current, I_{dc}, on DC bus due to inverter leg can be expressed as

$$I_{dc} = (u_1 u_4 - u_2 u_3)I_{inv} \quad (26)$$

The average state-space model of H-bridge inverter can be expressed as

$$\frac{dI_{inv}}{dt} = \frac{1}{L_f}(V_{inv} - V_s) \quad (27)$$

$$\frac{dV_{dc}}{dt} = \frac{1}{C_{dc}}I_{dc} \quad (28)$$

Results and discussion

The proposed single-phase, two-stage grid-integrated PV system employing nonlinear loads with APF functionality is simulated and its operation under various conditions of climatic, grid, DC bus voltage and load is investigated. A single-phase grid supply of 110 V, 50 Hz is considered and is connected to the nonlinear load. The proposed simulation study components and design parameters are represented in Tables 2 and 3, respectively.

Table 3. List of parameters.

S. No	Parameters	Specifications/values
1.	Converter controller gain parameters K_1, K_2, K_3	1, 10, 1
2.	Feedback ratio, β	0.294
3.	Scaling factor, G_s	0.017
4.	Inverter control hysteresis band, δ	0.02 V
5.	DC bus voltage controller gain, K_p, K_i	0.01, 0.1

Pure shunt active power filtering mode

In the absence of PV energy ($P_{PV} = 0$), the grid-connected inverter enters into a pure shunt APF mode and resultant waveforms of grid source voltage in volts, grid source current in amperes, load current in amperes and filter current (inverter output current) in amperes are shown in Figure 4. The measured waveforms are under steady-state condition with the nonlinear load condition of $R_{d1} = 15\ \Omega$ and $L_d = 3$ mH. Figure 4 illustrates that the grid source current is of the same shape as the grid source voltage and is in phase with it. The power factor measured under this condition is nearly unity.

The resultant real and reactive power obtained in grid source side, load side and inverter output side is shown in Figure 5. The real and reactive power profile obtained is illustrated in Table 4. The harmonic profile of the proposed PV-APF combination system is represented in Table 5. The total harmonic distortion (THD) of grid source voltage, grid source current and load current obtained during steady state is 1.31%, 1.72% and 85.12%, respectively. Figure 6 shows the response of the grid source current, source voltage, load current, inverter output current (filter current) and DC bus voltage with step change in nonlinear load condition at $t = 2$ s. These responses illustrate that irrespective of the nonlinearity of load changes, load type and presence of distortions in load current, the grid supply is close to sinusoidal and free from distortions. The measured THD of the grid supply (voltage and current) is less than 5% which meets the specified limits of the IEEE-519 harmonic standard. At a period $t = 2$ s, the step change in load occurs from 360 to 720 W and the response of DC bus voltage is lightly perturbed and settled with a maximum time period of 0.2 s.

Real power supply with shunt active power filtering mode (PV-APF integration system)

In the presence of PV energy ($P_{PV} < P_{Load}$ or $P_{PV} > P_{Load}$), the grid-connected inverter enters into a real power supply with shunt APF mode and resultant waveforms of grid source voltage in volts, grid source current in amps, load current in amps and filter current in amps are shown in Figure 7 employing fixed-frequency SMC-MPPT DC-DC converter. Figure 7
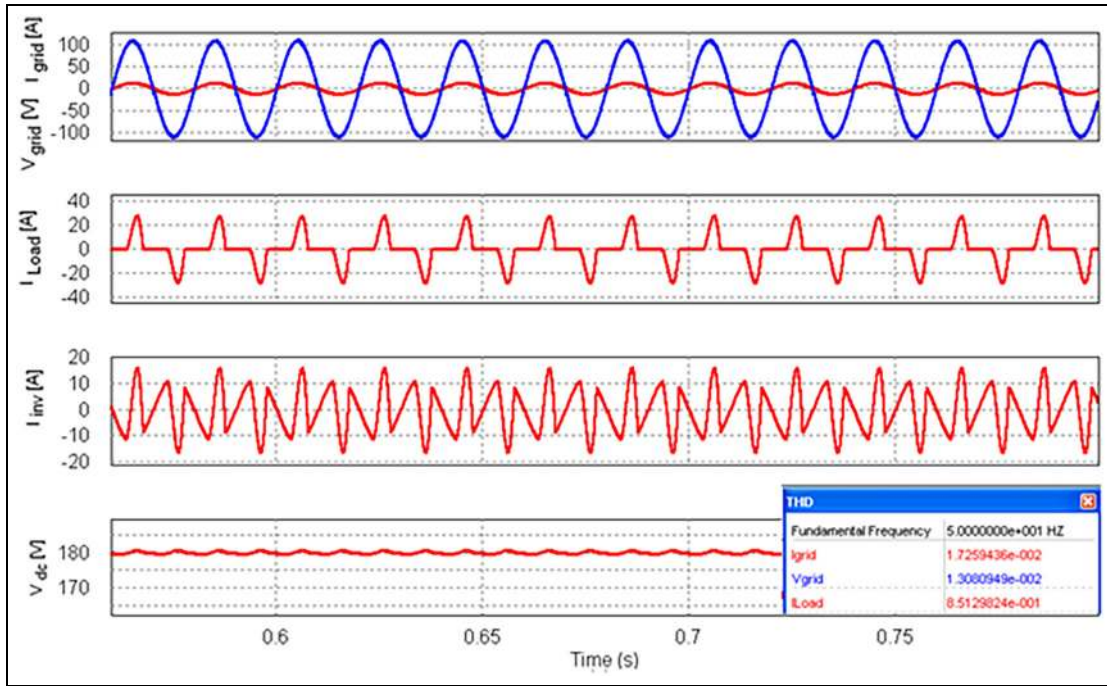
Figure 4. Resultant waveforms of grid source voltage, grid source current, load current and inverter output current during steady state (R_d = 15 Ω and L_d = 3 mH).
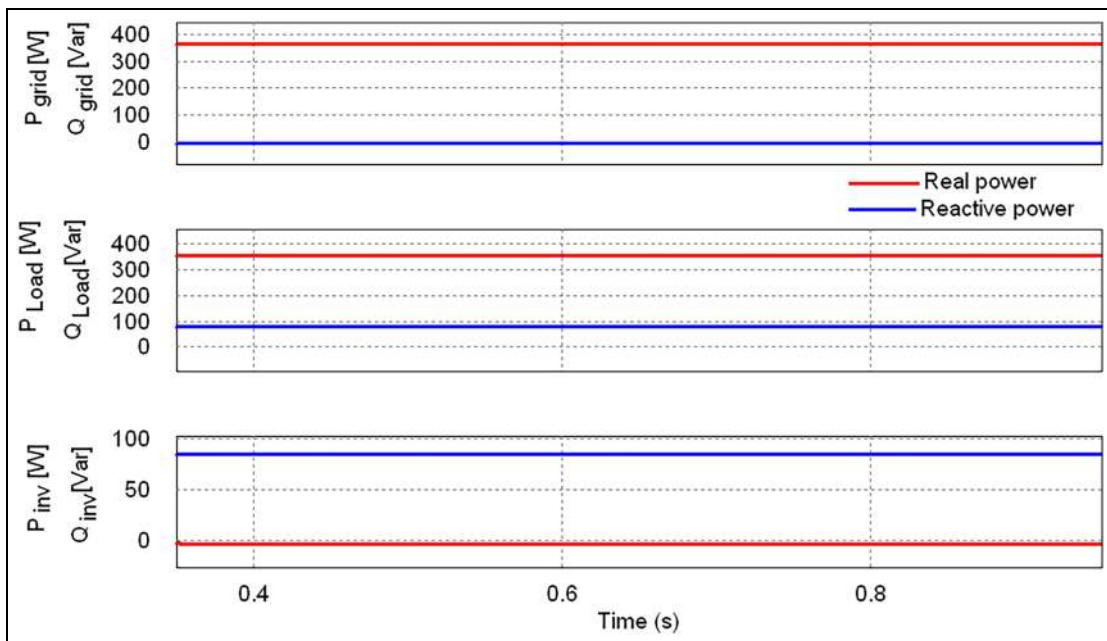

Figure 5. Real and reactive power profile in shunt active power filtering mode.

illustrates that the grid source current is of the same shape as the grid source voltage and is in phase with it. Figure 7 shows the effectiveness of the proposed fixed-frequency SMC-MPPT DC-DC converter connected with grid inverter employing nonlinear loads up to t = 0.6 s and an irradiance of 900 W/m² on the PV module. Figure 8 shows the response of source current, DC bus voltage, PV voltage and PV current with perturbation in irradiance.

The real and reactive power profile obtained in this case is illustrated in Figure 9. For this condition, the power consumed by the load is 360 W and the power supplied by the PV module is 81 W and the balance power 279 W is derived from the grid. The reactive power consumed by the load is supplied by the grid inverter. The harmonic profile of the proposed condition of PV-APF combination system under steady state is shown in Table 5. The THD of supply voltage, supply

Table 4. Real and reactive power profile.

Operating modes	Real power profile P (Watts)			Reactive power profile Q (VAr)		
	Grid (P_{grid})	Load (P_{Load})	Inverter (P_{inv})	Grid (Q_{grid})	Load (Q_{Load})	Inverter (Q_{inv})
Shunt APF	360	360	0 (absorb 2 W to meet loss)	0	90	90
Real power supply with APF (fixed-frequency SMC-MPPT)	279	360	81	0	90	90
Real power supply with APF (variable-frequency SMC-MPPT)	282.5	360	77.5	0	90	90

APF: active power filter; SMC-MPPT: sliding mode controller–maximum power point tracking.

Table 5. Measurement of THD in PV-APF integration system.

Operating modes	THD (%)		
	Grid supply voltage	Grid supply current	Load current
Case I: Nonlinear load $R_d = 15\ \Omega$ and $L_d = 3$ Mh			
Without APF filtering	14.09	84.82	84.82
Shunt APF mode	1.30	1.72	85.12
Real power supplier with APF mode (fixed-frequency SMC-MPPT)	0.818	1.56	85.09
Real power supplier with APF mode (variable-frequency SMC-MPPT)	0.90	2.46	85.32
Case II: Nonlinear load $R_d = 30\ \Omega$			
Without APF filtering	9.62	98.22	98.22
Shunt APF mode	1.26	2.0	98.13
Real power supplier with APF mode (fixed-frequency SMC-MPPT)	0.44	2.06	98.14
Real power supplier with APF mode (variable-frequency SMC-MPPT)	0.47	3.20	98.24
Case III: Nonlinear load $R_d = 15\ \Omega$			
Without APF filtering	14.09	84.82	84.82
Shunt APF mode	1.44	1.7	85.09
Real power supplier with APF mode (fixed-frequency SMC-MPPT)	0.78	1.55	85.06
Real power supplier with APF mode (variable-frequency SMC-MPPT)	0.88	2.44	85.28

THD: total harmonic distortion; APF: active power filter; SMC-MPPT: sliding mode controller–maximum power point tracking.
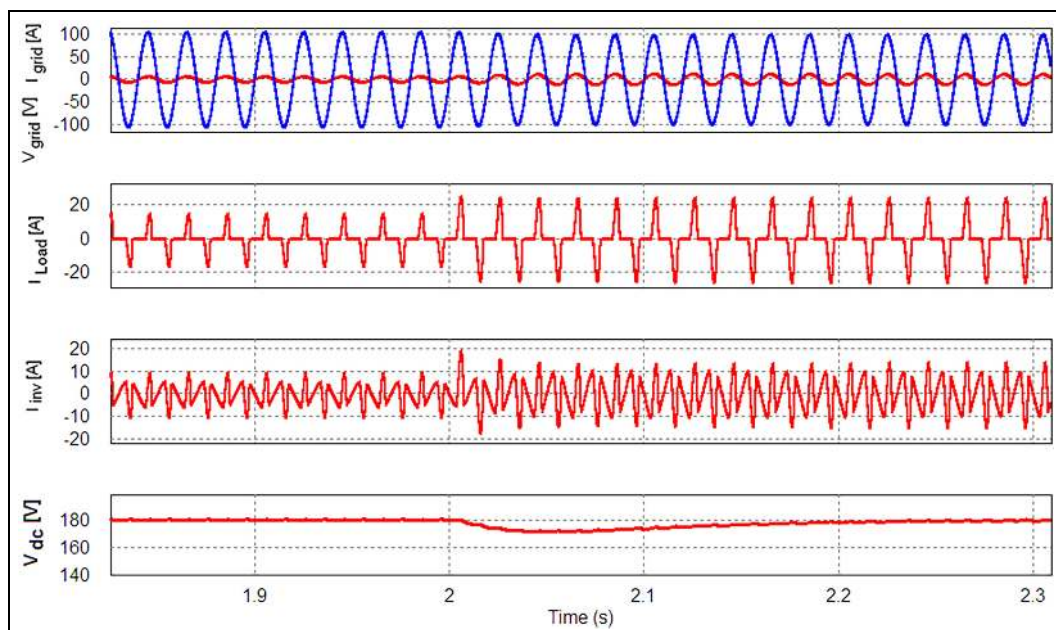

Figure 6. Dynamic response of source current, inverter output current and DC bus voltage with step variation of load ($R_d = 30\ \Omega$ to $R_d = 15\ \Omega$ and $L_d = 3$ mH).
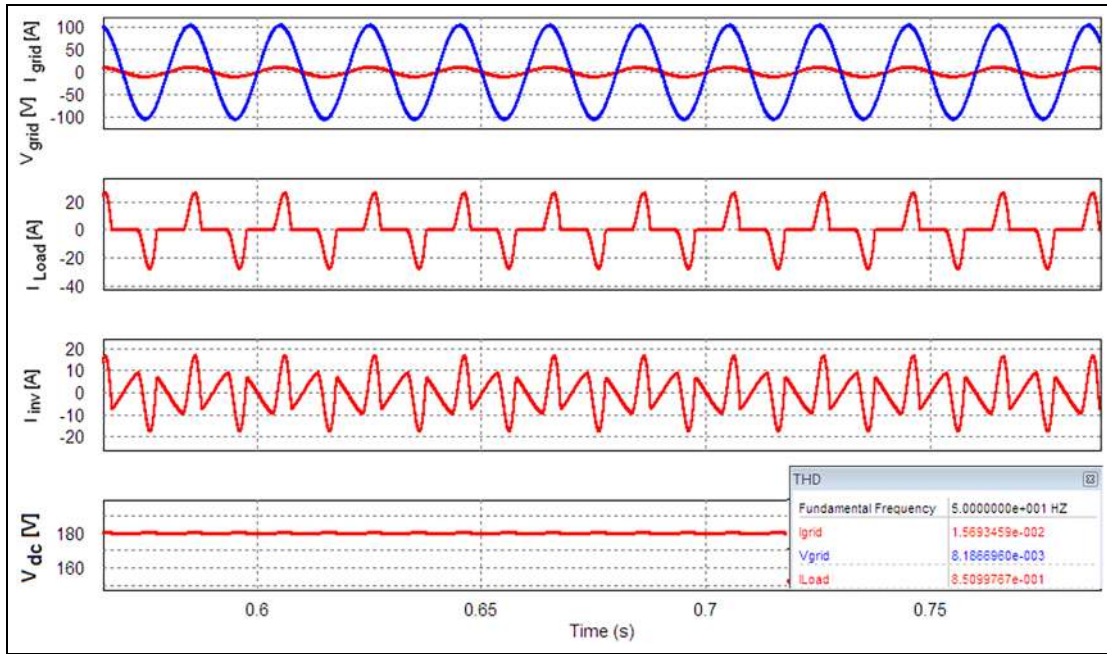
Figure 7. Waveforms of grid source voltage, grid source current, load current, inverter output current and DC bus voltage with fixed-frequency SMC-MPPT operation during steady state (R_{d1} = 15 Ω and L_d = 3 mH).
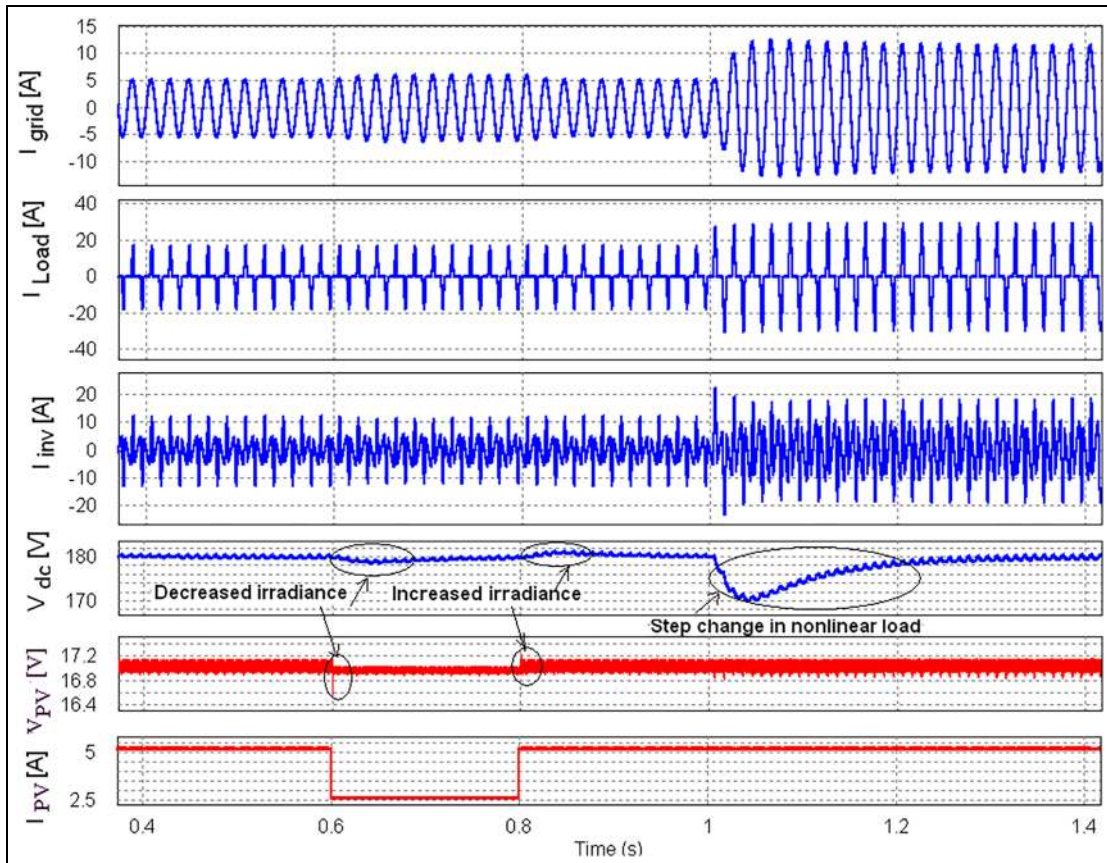

Figure 8. Dynamic response of grid source current, load current, inverter output current, DC bus voltage, PV voltage and PV current with perturbation in irradiance and step variation of nonlinear load (R_d = 30 Ω to R_{d1} = 15 Ω and L_{d1} = 3 mH).

current and load current obtained is 0.818%, 1.56% and 85.09%, respectively. Also, it illustrates that irrespective of the nonlinearity of load changes, load type and presence of distortions in load current, the grid supply is close to sinusoidal and free from distortions. The measured THD of the grid supply is less than 5%
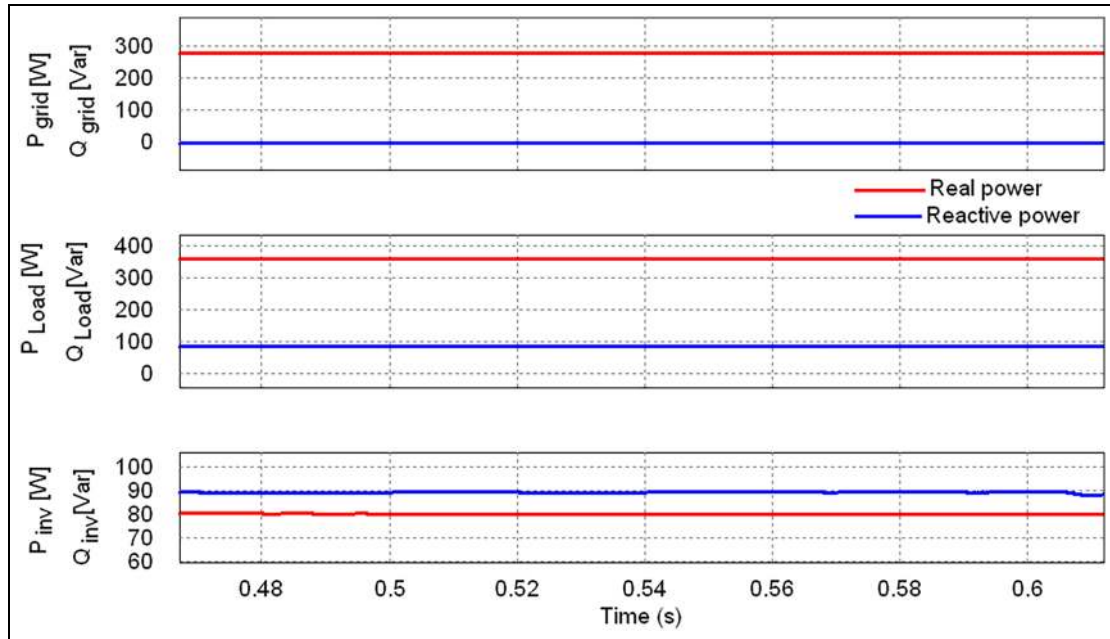
Figure 9. Real and reactive power profile in real power supply with shunt active power filtering mode.
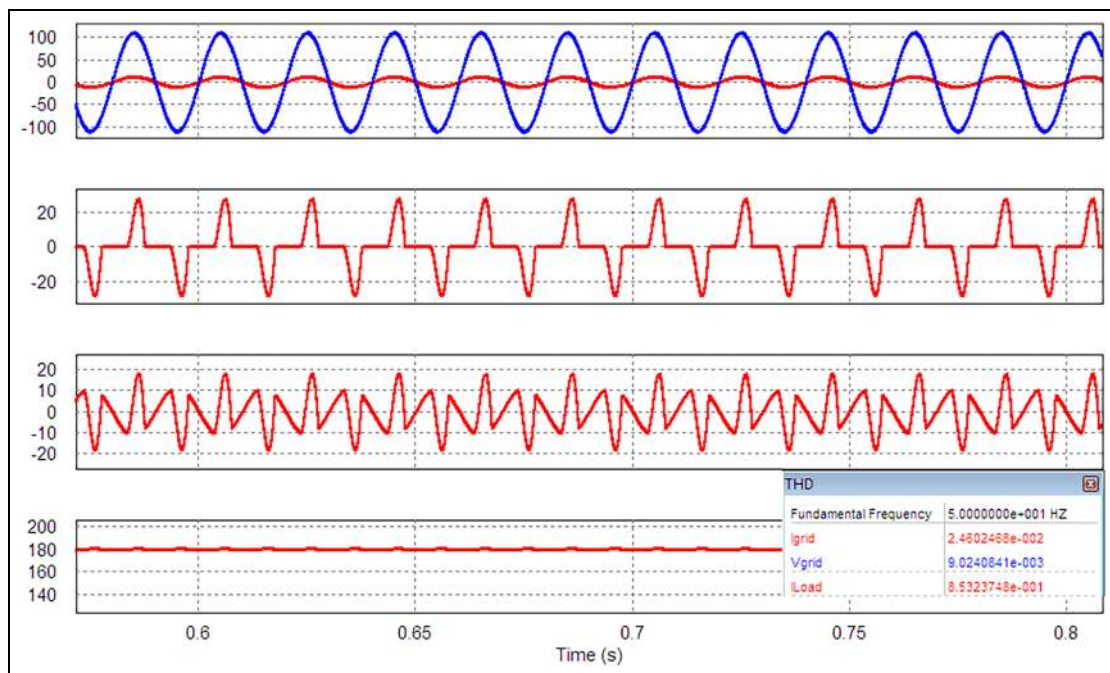

Figure 10. Resultant waveforms of grid source voltage, grid source current, load current, inverter output current and DC bus voltage with variable-frequency SMC-MPPT operation during steady state (R_{d1} = 15 Ω and L_{d1} = 3 mH).

which meets the specified limits of the IEEE-519 harmonic standard.

At a period t = 0.6 s (see Figure 8), irradiance is suddenly varied from 900 to 450 W/m². Under this condition, the power supplied by the PV module is 40 W and the balance power 320 W is derived from the grid. At a period t = 0.8 s (see Figure 8), again irradiance is suddenly changed from 450 to 900 W/m². It is noted that the DC-link voltage under this condition of sudden

change in irradiance level is regulated after a period of t = 0.05 s. At a period t = 1 s, the step change in load occurs from 360 to 720 W, the response of DC bus voltage is lightly perturbed and settled with a maximum time period of 0.2 s but the PV voltage is still regulated which illustrates the proficiency of the proposed control system (see Figure 8).

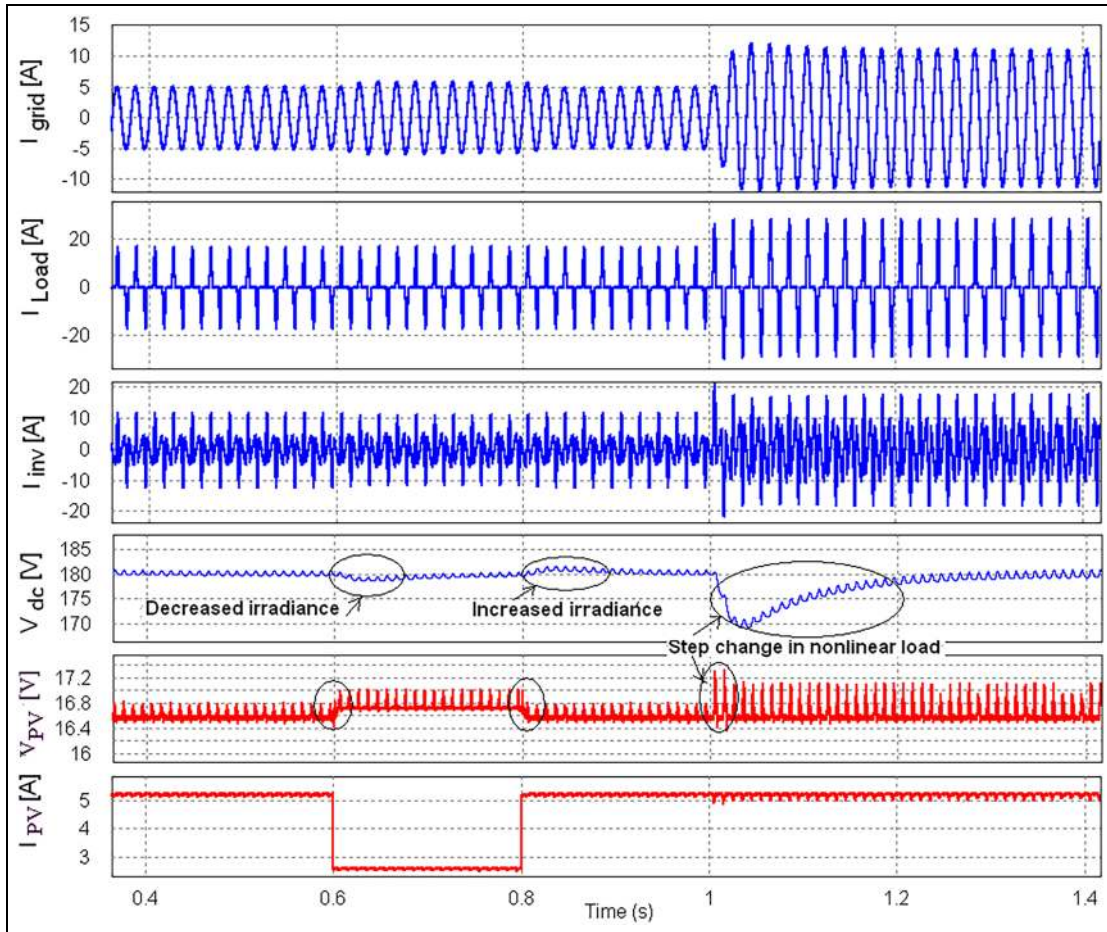The decrease and increase in the value of PV power at DC-link is conformed through decrease and increase

Figure 11. Dynamic response of grid source current, load current, inverter output current, DC bus voltage, PV voltage and PV current with perturbation in irradiance and step variation of nonlinear load ($R_d = 30\,\Omega$ to $R_{d1} = 15\,\Omega$ and $L_{d1} = 3\,mH$).
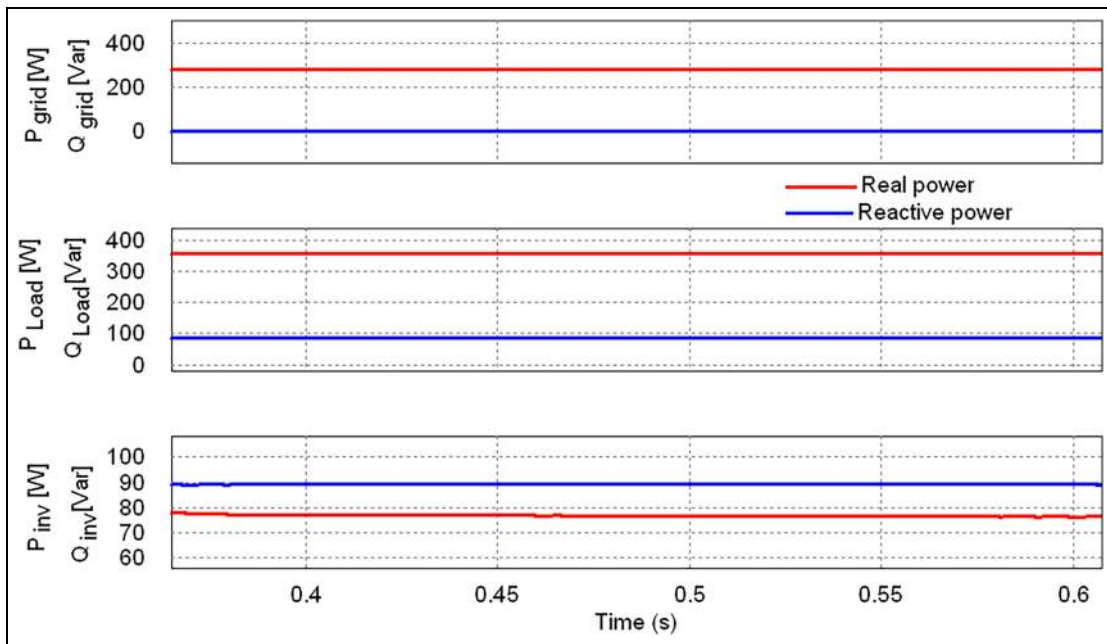

Figure 12. Real and reactive power profile under variable frequency hysteresis-based SMC-MPPT.

**Table 6.** Comparison results of two controllers for PV-MPPT application (MPPT and grid efficiency).

Controller	Grid-connected PV system				
	Theoretical true PV power (W)	Tracked PV power (W)	MPPT efficiency (%)	Injected grid power (W)	Grid efficiency
Variable-frequency SMC	90	86.25	95.83	77.5	89.85
Fixed-frequency SMC	90	89.25	99.16	81	90.75

PV: photovoltaic; MPPT: maximum power point tracking; SMC: sliding mode controller.

Table 7. Comparison results of two controllers with PV-MPPT application (settling time, chattering magnitude and peak overshoot).

Controller	Simulation analysis			Experimental analysis		
	Settling time (s)	Chattering magnitude (V) (h_1–h_2)	Peak overshoot (%)	Settling time (s)	Chattering magnitude (V) (h_1–h_2)	Peak overshoot (%)
Variable-frequency SMC	0.03	0.15	7.11–8.28	0.04–0.08	1	11.56
Fixed-frequency SMC	0.0008–0.001	0.11–0.14	4.71	0.008–0.03	0.5	5.88

SMC: sliding mode controller.
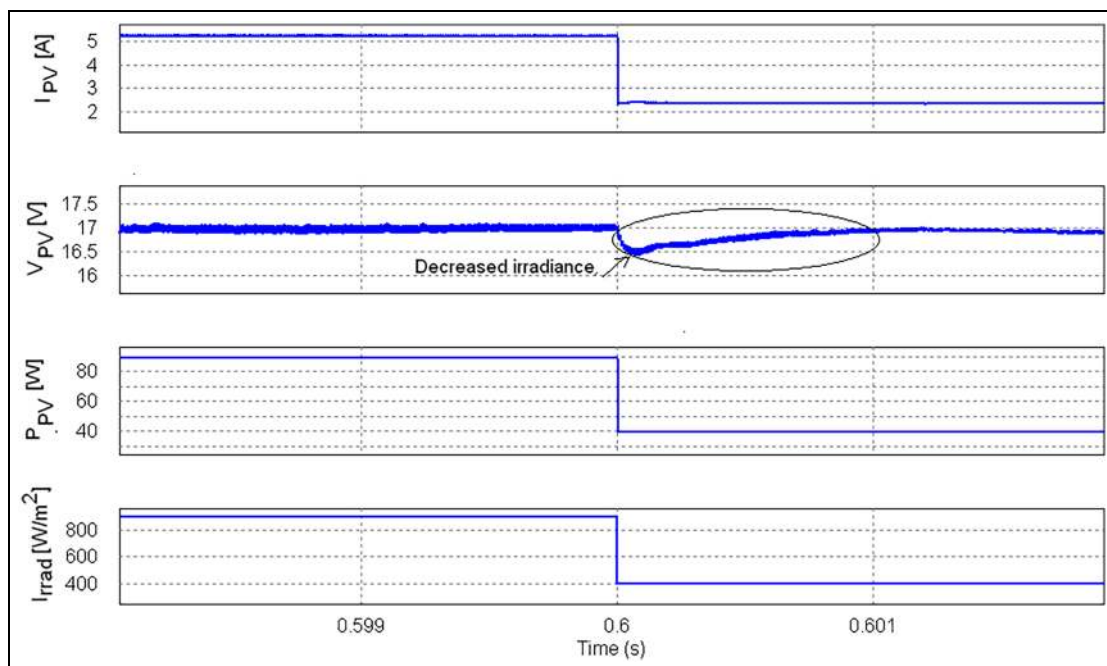
Figure 13. Simulated transient response of PV current, PV voltage and PV power with variable irradiance using fixed-frequency SMC-MPPT operation.

in the value of injected inverter output current represented in Figure 8. Then, the corresponding increase and decrease in the magnitude of grid source current is characterized (see Figure 8). This represents that the grid inverter can be controlled to make it function as both real power supplier and shunt APF and mitigate power quality problems. Suitable control has been implemented for the grid-integrated PV system to extract maximum real power and to meet the reactive power demand of the system.

Figures 10–12 show the effectiveness of the variable-frequency hysteresis-based SMC-MPPT boost converter connected with grid environment employing nonlinear loads. From the results, it is to be found that the transition from different operating regions is characterized but the PV voltage is not well regulated fast (see Figure 10). The dynamic and steady-state response of the PV system is poor and introduces more chattering magnitude and the maximum available PV power is not fully transferred to grid. The comparison results of
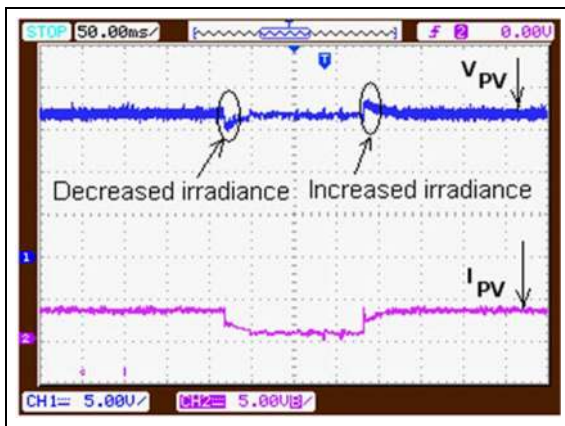
Figure 14. Experimental response of PV current and PV voltage with fast irradiance variation (fixed-frequency PWM-based SMC-MPPT operation).
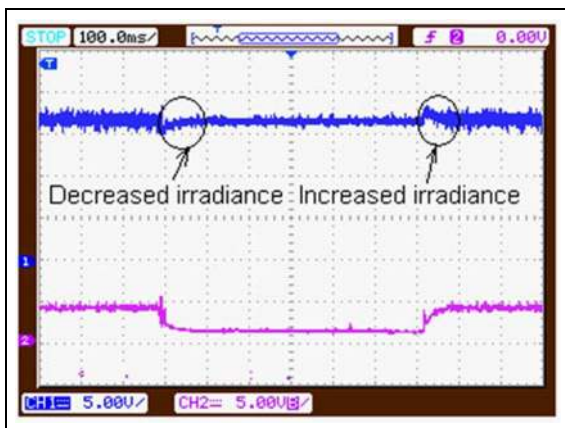

Figure 15. Experimental response of PV current and PV voltage with fast irradiance variation (variable-frequency hysteresis-based SMC-MPPT operation).

both the systems are illustrated in Tables 6 and 7, respectively. The harmonic profile of the proposed PV-APF combination system is shown in Table 5. The THD of supply voltage, supply current and load

current obtained is 0.90%, 2.48% and 85.32%, respectively, for the same load condition operated by the fixed-frequency PWM-based PV-APF combination system described previously.

Figure 13 shows the simulated response of PV current and PV voltage using fixed-frequency PWM-based SMC-MPPT with decreased value of irradiance from 900 to 400 W/m^2 at time t = 0.6 s. When the irradiance decreases, the PV current decreases simultaneously but the system voltage reaches a steady state after a small transient period of approximately 0.001 s maximum (see Figure 13). An experimental hardware prototype is constructed in laboratory in order to check the proficiency of the fixed-frequency SMC-MPPT converter operation.

Figure 14 shows the experimental behaviour of the PV voltage and current which is obtained by fast irradiance variation, which confirms the simulations presented in Figure 13. When the irradiance decreases or increases, the PV current decreases or increases simultaneously but the system voltage reaches a steady state after a small transient period of approximately 0.03 s (see Figure 14). Similarly, Figure 15 shows the experimental response of the PV voltage and current which is obtained by fast irradiance variation using variable-frequency SMC-MPPT converter. The response time is poor (0.08 s maximum) and introduces more chattering in this case (see Figure 15).

Figure 16 shows the generated gate pulse and corresponding PV voltage of variable- and fixed-frequency SMC-MPPT converter at the particular value of irradiation. Figure 16 illustrates that the variable-frequency SMC-MPPT introduces more chattering magnitude when compared to fixed-frequency SMC-MPPT. Table 7 illustrates the comparison results of two controllers with PV-MPPT application. The results are obtained under the condition of 900 to 200 W/m^2 with the temperature of 25 °C. As a result, the PV system with the proposed fixed-frequency SMC-MPPT maintains stability under all range of solar irradiance.
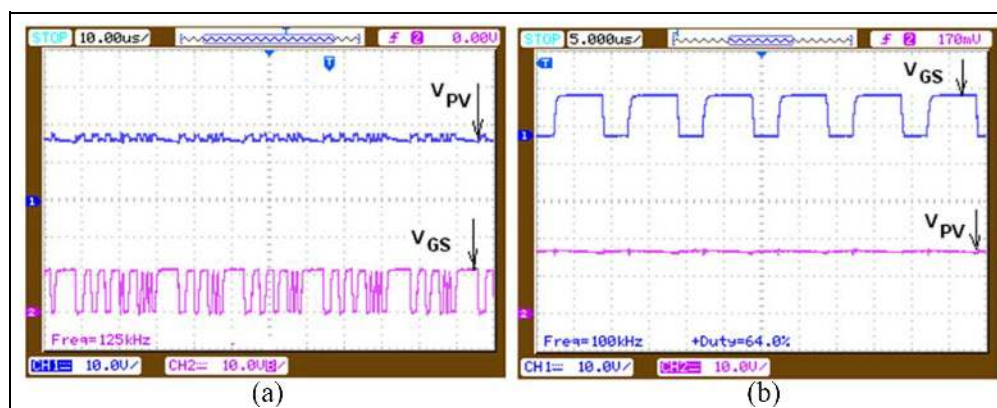

Figure 16. Gating signal and PV voltage: (a) variable-frequency hysteresis-based SMC-MPPT; (b) fixed-frequency PWM-based SMC-MPPT.

Conclusion

This article discusses the performance analysis of grid-integrated PV system employing nonlinear loads with fixed- and variable-frequency SMC-MPPT DC-DC converter. A simple nonlinear controller of grid inverter based on SMC not only meets the function of real power demand of load but also performs reactive power and harmonic compensation to the local load. Hence, the utility grid supplies a lesser real power demand and nearly negligible reactive power demand of the local load. This makes the grid supply current as nearly sinusoidal and harmonic free. The THD measured is within the limits of IEEE 519-1992 standards. The proficiency of the designed controller has been demonstrated against load and irradiance variations. The results of the SMC-MPPT boost converter have fast dynamic response in accordance with uncertainties in climatic and load conditions. The application of the proposed design of PV-APF combination system employing nonlinear load compensation is cost effective, simple to implement, innovative and found to work well for low- to medium-scaled two-stage grid-integrated PV system.

Declaration of conflicting interests

The author(s) declared no potential conflicts of interest with respect to the research, authorship and/or publication of this article.

Funding

The author(s) received no financial support for the research, authorship and/or publication of this article.

ORCID iD

Ravichandran Chinnappan 🔟 https://orcid.org/0000-0002-3326-418X

References

1. Bojoi R, Limongi L, Roiu D, et al. Enhanced power quality control strategy for single-phase inverters in distributed generation systems. *IEEE T Power Electr* 2011; 26(3): 798–806.
2. Mukhtiar S, Vinod K, Ambrish C, et al. Grid interconnection of renewable energy sources at the distribution level with power-quality improvement features. *IEEE T Power Deliver* 2011; 26(1): 307–315.
3. Yang B, Li W, Zhao Y, et al. Design and analysis of a grid-connected photovoltaic power system. *IEEE T Power Electr* 2010; 25(4): 992–1000.
4. Haroun R, El Aroudi A, Cid-Pastor A, et al. Impedance matching in photovoltaic systems using cascaded boost converters and sliding-mode control. *IEEE T Power Electr* 2015; 30(6): 3185–3199.
5. Tseng KC and Huang CC. High step-up high-efficiency interleaved converter with voltage multiplier module for renewable energy system. *IEEE T Ind Electron* 2014; 61(3): 1311–1319.
6. Sukesh N and Pahlevaninezhad M. Analysis and implementation of a single-stage flyback PV micro-inverter with soft switching. *IEEE T Ind Electron* 2014; 61(4): 1819–1833.
7. Femia N, Petrone G, Spagnuolo G, et al. A technique for improving P&O MPPT performances of double-stage grid-connected photovoltaic systems. *IEEE T Ind Electron* 2009; 56(11): 4473–4482.
8. Saxena H, Singh A and Rai JN. Design and performance analysis of generalised integrator-based controller for grid connected PV system. *Int J Electron* 2018; 105(7): 1079–1096.
9. Kim I-S, Kim M-B and Youn M-J. New maximum power point tracker using sliding-mode observer for estimation of solar array current in the grid-connected photovoltaic system. *IEEE T Ind Electron* 2006; 53(4): 1027–1035.
10. Jain S and Agarwal V. Comparison of the performance of maximum power point tracking schemes applied to single-stage grid-connected photovoltaic systems. *IET Electr Power App* 2007; 1(5): 753–762.
11. Tuyen ND and Fujita G. PV-active power filter combination supplies power to nonlinear load and compensates utility current. *IEEE Pow Ener Tech Syst J* 2015; 2(1): 32–42.
12. Bianconi E, Calvente J, Giral R, et al. A fast current-based MPPT technique employing sliding mode control. *IEEE T Ind Electron* 2013; 60(3): 1168–1178.
13. Jiang W, Chincholkar SH and Chan CY. Comparative study of adaptive current-mode controllers for a hybrid-type high-order boost converter. *IET Power Electron* 2017; 11(3): 524–530.
14. Chincholkar SH and Chan C-Y. Design of fixed-frequency pulse-width-modulation-based sliding-mode controllers for the quadratic boost converter. *IEEE T Circuits Syst* 2017; 64(1): 51–55.
15. Tan SC, Lai YM, Cheung KH, et al. On the practical design of a sliding mode voltage controlled buck converter. *IEEE T Power Electr* 2005; 20(2): 425–437.
16. Tan SC, Lai YM and Tse CK. A unified approach to the design of PWM-based sliding-mode voltage controllers for basic DC-DC converters in continuous conduction mode. *IEEE T Circuits: I* 2006; 53(8): 1816–1827.
17. IEEE Standard 519:1992. IEEE recommended practices and requirements for harmonic control in electric power systems (ANSI).
18. Baek J-W, Ryoo M-H, Kim T-J, et al. High boost converter using voltage multiplier. In: *Proceedings of the 31st annual conference of IEEE Industrial Electronics Society 2005 (IECON 2005)*, Raleigh, NC, 6–10 November 2005. New York: IEEE.
19. Li W and He X. Review of non-isolated high-step-up DC/DC converters in photovoltaic grid-connected applications. *IEEE T Ind Electron* 2011; 58(4): 1239–1250.
20. Knabben GC, Schmitz L, Custodio OJ, et al. Photovoltaic micro-inverter with active filtering and thin-film capacitors. In: *Proceedings of the 2017 Brazilian power electronics conference (COBEP)*, Juiz de Fora, 19–22 November 2017, pp. 1–6. New York: IEEE.
21. Bezerra MA, Oliveira JL, Praça PP, et al. Proposal of a control scheme for an active filter on PV micro-inverter applications. In: *Proceedings of the applied power electronics conference and exposition (APEC)*, Tampa, FL, 26–30 March 2017, pp. 2830–2837. New York: IEEE.

22. Torrey DA and Al-Zamel AMAM. Single-phase active power filters for multiple nonlinear loads. *IEEE T Power Electr* 1995; 10(3): 263–272.

23. Dong D, Boroyevich D, Mattavelli P, et al. A high performance single-phase phase-locked-loop with fast line-voltage amplitude tracking. In: *Proceedings of the 2011 26th annual IEEE applied power electronics conference and exposition (APEC)*, Fort Worth, TX, 6–11 March 2011, pp. 1622–1628.

24. Thacker T, Boroyevich D, Burgos R, et al. Phase-locked loop noise reduction via phase detector implementation for single-phase systems. *IEEE T Ind Electron* 2011; 58(6): 2482–2490.

25. Karimi-Ghartemani M. A unifying approach to single-phase synchronous reference frame PLLs. *IEEE T Power Electr* 2013; 28(10): 4550–4556.

26. Lee KJ, Lee JP, Shin D, et al. A novel grid synchronization PLL method based on adaptive low-pass notch filter for grid-connected PCS. *IEEE T Ind Electron* 2014; 61(1): 292–301.

27. Golestan S, Freijedo FD, Vidal A, et al. An efficient implementation of generalized delayed signal cancellation PLL. *IEEE T Power Electr* 2016; 31(2): 1085–1094.

28. Konstantopoulos GC, Zhong QC and Ming WL. PLL-less nonlinear current-limiting controller for single-phase grid-tied inverters: design, stability analysis and operation under grid faults. *IEEE T Ind Electron* 2016; 63(9): 5582–5591.

29. Chen X, Zhang Y, Wang S, et al. Impedance-phased dynamic control method for grid-connected inverters in a weak grid. *IEEE T Power Electr* 2017; 32(1): 274–283.

30. Jaume M, De Vicuna LG, Miguel C, et al. Design of an analog quasi-steady-state nonlinear current-mode controller for single-phase active power filter. *IEEE T Ind Electron* 2009; 56(12): 4872–4881.